Snowmelt on the Greenland Ice Sheet as Derived from Passive Microwave Satellite Data

WALEED ABDALATI AND KONRAD STEFFEN

Center for the Study of Earth from Space, Cooperative Institute for Research in Environmental Sciences, University of Colorado, Boulder, Colorado

(Manuscript received 1 December 1995, in final form 29 April 1996)

ABSTRACT

The melt extent of the snow on the Greenland ice sheet is of considerable importance to the ice sheet's mass and energy balance, as well as Arctic and global climates. By comparing passive microwave satellite data to field observations, variations in melt extent have been detected by establishing melt thresholds in the cross-polarized gradient ratio (XPGR). The XPGR, defined as the normalized difference between the 19-GHz horizontal channel and the 37-GHz vertical channel of the Special Sensor Microwave/Imager (SSM/I), exploits the different effects of snow wetness on different frequencies and polarizations and establishes a distinct melt signal. Using this XPGR melt signal, seasonal and interannual variations in snowmelt extent of the ice sheet are studied. The melt is found to be most extensive on the western side of the ice sheet and peaks in late July. Moreover, there is a notable increasing trend in melt area between the years 1979 and 1991 of 4.4% per year, which came to an abrupt halt in 1992 after the eruption of Mt. Pinatubo. A similar trend is observed in the temperatures at six coastal stations. The relationship between the warming trend and increasing melt trend between 1979 and 1991 suggests that a 1°C temperature rise corresponds to an increase in melt area of 73 000 km^2, which in general exceeds one standard deviation of the natural melt area variability.

1. Introduction

The Greenland ice sheet is one of the major ice sheets of the world and as such plays an important role in the global and regional climates. With a present surface area of 1.75×10^6 km^2 and a volume of 2.65×10^6 km^3, which correspond to 11% and 8% of the global glacier surface area and ice volume, respectively (Thomas 1993), it contains enough water to raise the current sea level by 7 m (Warrick and Oerlemans 1990). As a result, it can potentially play a significant role in sea level change.

Of major climatological significance is the areal extent and duration of surface snowmelt on the ice sheet. Because wet snow absorbs significantly more incident solar radiation than dry snow, the ice sheet composes an unstable, positive feedback component of the climate system. That is to say that an increase in snowmelt on the ice sheet will result in the absorption of more of the incident solar energy, which will, in turn, cause further melting and so on. In addition, increased melt can contribute to cloud feedback, as melting snow provides a vapor source for cloud formation, which, in turn, will increase the downwelling longwave radiation, which can further increase melt. Thus, the instability of the ice sheet due to snowmelt may be much greater than the simple albedo effect. The assessment of these cloud feedback effects is beyond the scope of this paper; however, they do underscore the importance of understanding ice sheet melt characteristics.

Because of the large size and gentle slope of most of the Greenland ice sheet, small changes in the air temperature will result in large areal changes in the dry and wet snow facies. Assuming an adiabatic lapse rate of 0.6°C/100 m (Orvig 1970), a slope above the equilibrium line of 0.4° (Steffen 1995), and a melt area perimeter of 3300 km, a 1°C temperature rise will increase the melt area by 79 000 km^2. Therefore, it is evident that the melt conditions are a very sensitive parameter in the Arctic climate and climate changes.

To understand the role of melt in the climate variability, and the impact of the climate on ice sheet melt extent, a means of monitoring the melt characteristics of the ice sheet over large areas and long periods of time is necessary. Because of the remoteness and unfavorable environment on the ice sheet, the in situ data are very limited. For this reason spaceborne in-

Corresponding author address: Dr. Waleed Abdalati, Universities Space Research Association, NASA/Goddard Space Flight Center, Mail Code 972.0, Greenbelt, MD 20771.
E-mail: abdalati@osb.wff.nasa.gov

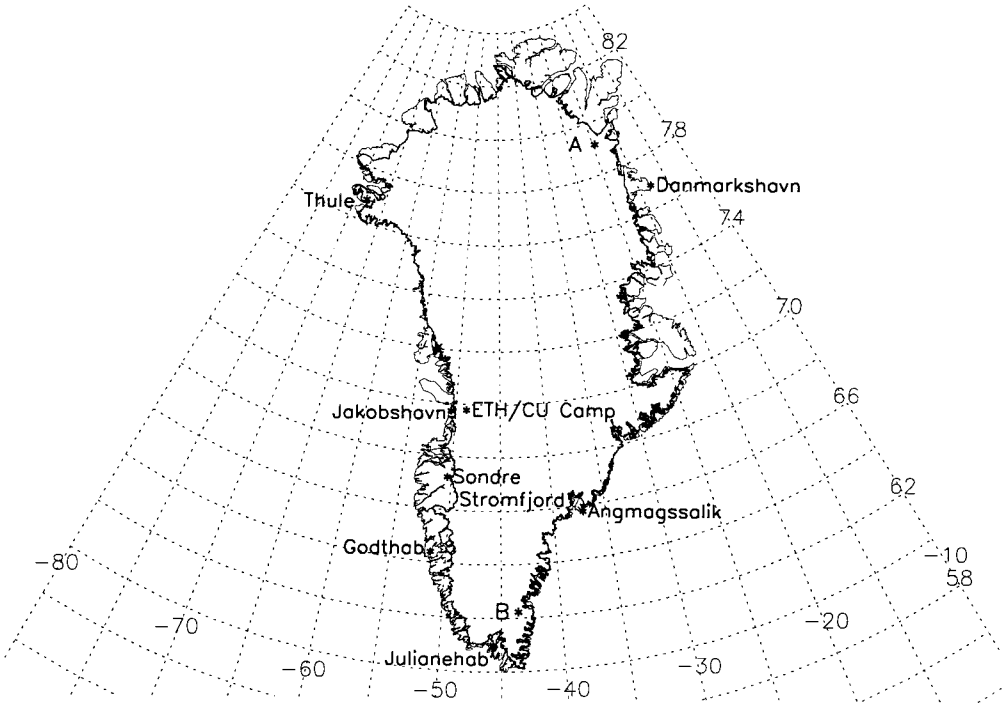

FIG. 1. Location map of the Greenland ice sheet. The thin line represents the coastal outline, while the thicker line represents the ice sheet perimeter. The figure includes the location of the ETH/CU camp, the six climate stations from which the coastal temperature data were used, and the locations (A and B) for which XPGR time series were analyzed previously by Abdalati and Steffen (1995).

struments can provide extensive datasets for the region. Passive microwave data are particularly well suited for such observations for several reasons: 1) microwave emission changes dramatically when liquid water forms in the snow for frequencies greater than 10 GHz (Ulaby et al 1986), 2) microwave radiation can penetrate clouds, and 3) coverage in the Arctic is frequent with these wide-swath instruments.

In this study, the passive microwave based method of Abdalati and Steffen (1995) for detecting melt extent is used to study the seasonal and interannual variations of melt on the ice sheet. The behavior of the Greenland ice sheet in the recent past is examined, and comparisons are made to climatological data from coastal climate stations. The objective is to characterize the ice sheet melt, identify melt trends, and understand the relationships between changes in the climate and changes in the ice sheet melt characteristics.

2. Data

a. Passive microwave satellite data

The satellite data used for this analysis are from the Scanning Multichannel Microwave Radiometer (SMMR), which was operational from October 1978 through August 1987, and the Special Sensor Microwave/Imager (SSM/I), which has been operational since July 1987. Data from two SSM/I sensors were used in this study. For the period of 9 July 1987 through 31 December 1991, the SSM/I instrument on the Defense Meteorological Satellite Program (DMSP) *F-8* satellite was used, and for the remainder of the study period, 1 January 1992 through 31 August 1994, data from the DMSP *F-11* SSM/I instrument were used. Because of the differing orbital characteristics of the two instruments and the fact that the SMMR instrument has vertical and horizontal 18-GHz channels instead of the 19-GHz channels on the SSM/I, all of the instruments had to be cross-calibrated. This was accomplished by using the coefficients of Jezek et al. (1991) for the SMMR data, and those of Abdalati et al. (1995) for the SSM/I *F-11* data. The SSM/I *F-8* data were taken as the baseline dataset and as such required no adjustments (Abdalati et al. 1995).

The SMMR and SSM/I data for this analysis were provided on CD-ROM by the National Snow and Ice Data Center (NSIDC) in Boulder, Colorado. These satellite data sets are arranged in a 25 km × 25 km grid scale and binned into averages for every day of coverage. The SSM/I data are available for nearly every day of the coverage period, while the SMMR data are available only for nearly every other day of the period (SMMR was only operational every other day). These

data compose a comprehensive and continuous multichannel dataset for the years 1979–94.

b. In situ data

In the spring of 1990 scientists from the Swiss Federal Institute of Technology (ETH) in Zurich installed a semipermanent research camp at the equilibrium line of the Greenland ice sheet near Jakobshavn (see Fig. 1). The exact location of the Swiss camp (also called the ETH/CU camp since its transfer to the University of Colorado in 1992) is at 69°34′N lat and 49°17′W long, and 1150 m above sea level. Since its establishment, the station has provided a full suite of climatological data including temperatures below and above the ice, radiation data, atmospheric data, information on snow properties throughout the transition from dry to wet snow, radiosonde data, measurements pertaining to the ice flow dynamics, and other useful information about this data-sparse area.

While all of the data provide critical pieces to the complex puzzle of the Greenland climate, of particular interest in this study are the snow data collected during the transitions of the snow from dry to wet. Because of the different participants, project emphases, and times of occupation each year, the datasets at the camp differ slightly from year to year. In the 1990, 1991, 1993, and 1995 field seasons, wetness measurements were determined from dielectric constant measurements made with a Flatsensor B85 PSI 873 instrument (Denoth 1985) at 5–10-cm intervals (depending on the presence of ice lenses) in the snow, and an average wetness was calculated. During the 1992 field season melt assessment was not a part of the field plan, and no measurements were made. In the spring of 1994, melt occurred late in the season after camp closure, so no measurements were made of the water content. However, temperature measurements were made in absentia at various levels in the snow, which provided a proxy for an estimate of melt onset. These data have been the basis for algorithm validation (Abdalati and Steffen 1995) and melt climatology.

3. Method

a. Passive microwave melt signal

During the transition from dry snow to wet snow the microwave emissivity of the snow increases dramatically as surface scattering begins to dominate over volume scattering (Mätzler and Hüppi 1989). For passive microwave observations, this sharp increase is evident in the brightness temperature signal in accordance with the Rayleigh–Jeans approximation for radiation in the microwave part of the electromagnetic spectrum:

$$T_b(\lambda) = \epsilon T_p, \tag{1}$$

where T_b refers to the microwave brightness temperature at a particular wavelength (λ), ϵ is the microwave emissivity, and T_p is the effective physical temperature of the snow (Zwally 1977). These brightness temperature increases are frequency and polarization dependent (Ulaby et al. 1986).

Changes in microwave emission during snowmelt have been used by Steffen et al. (1993), Mote et al. (1993), and Mote and Anderson (1995) to study the spatial and temporal extent of melt on the Greenland ice sheet based on SMMR and SSM/I observations. Zwally and Fiegles (1994) and Ridley (1993) also have used them to investigate the melt extent in Antarctica using SMMR and SSM/I data as well. With the exception of Steffen et al., each of these methods is based on the change in emission for a single microwave channel and polarization. Mote et al, (1993), Zwally and Fiegles (1993), and Ridley (1993) use the 19-GHz vertically polarized channel (19V) for the SSM/I data and the 18-GHz vertical polarization (18V) for the SMMR data. Mote and Anderson use the 37-GHz horizontally polarized channel (37H) for both instruments. Steffen et al. based their method on a normalized difference between the 19-GHz horizontal (19H) channel and the 37H channel.

In this study, the cross-polarized gradient ratio technique of Abdalati and Steffen (1995), with a slight modification, is used to classify wet and dry snow. This method utilizes both the frequency and polarization dependence of snow emission on liquid water content. Lower microwave frequencies, such as 19 GHz, are more responsive to melt onset in the firn, than are higher frequencies, such as 37 GHz (Steffen et al. 1993). This is primarily due to the change in emission depth (extinction characteristics) associated with melt. The polarization dependence is such that small amounts of water in the snow cause a greater increase in horizontal brightness temperatures than vertical brightness temperatures at the same frequency. This depolarization effect arises due to the change in dielectric properties at the air–snow interface when snow is wet.

Combining the frequency- and polarization-dependent response to melt yields a combination of channels for the classification of wet and dry snow. It is referred to as the cross-polarized gradient ratio (XPGR):

$$\text{XPGR} = \frac{T_b(19\text{H}) - T_b(37\text{V})}{T_b(19\text{H}) + T_b(37\text{V})}. \tag{2}$$

Using this relationship, a threshold can be defined based on which ice sheet melt extent is identified, mapped, and monitored in both space and time. A time series of the XPGR of the Swiss camp for the dates of SSM/I coverage is shown in Fig. 2 along with the dates of observed melt onset. The thresholds for each instrument are also shown.

Prior to analysis of ice sheet melt conditions, an ice mask was applied to extract only the pixels that lie entirely on the ice sheet. This mask was generated from

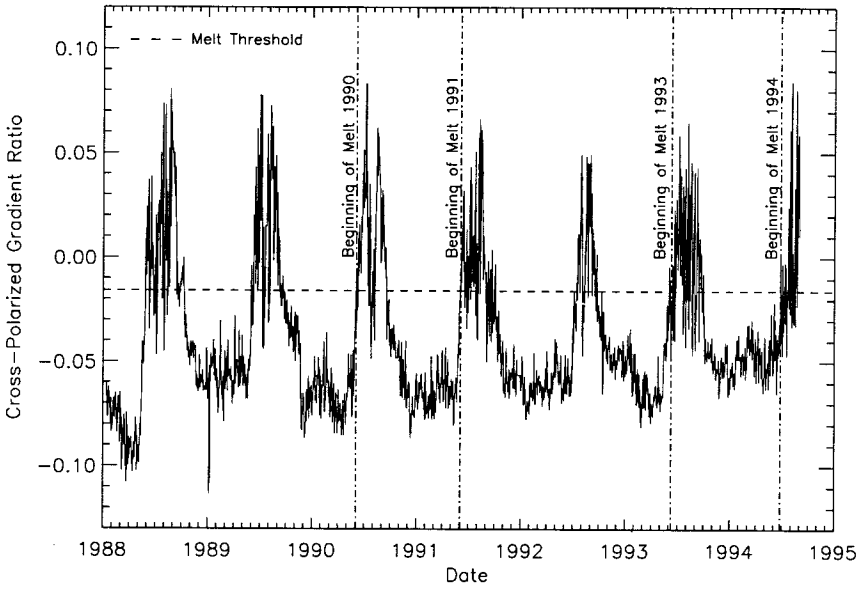

FIG. 2. Cross-polarized gradient ratio (XPGR) time series for the ETH/CU camp pixel for the dates of available SSM/I data. Also shown are the dates on which melt was observed to begin at the camp and the corresponding XPGR threshold (XPGR = −0.158) associated with melt.

digitization of the Quaternary Map of Greenland produced by the Geological Survey of Greenland (1: 2 500 000 scale). Pixels with any portion outside the ice sheet were not included because mixed pixels of land and ice would give erroneous melt results. As a result, approximately 6% of the ice sheet is eliminated from the analysis. This 6%, since it is at low elevations along the perimeter, is believed to experience some melt, but it is omitted from this study.

b. SSM/I F-8 *analysis*

The data initially analyzed in this study were the SSM/I data from 1 January 1988 through 31 December 1991. For each of the ice pixels, the cross-polarized gradient ratio was calculated according to Eq. (2) and a time series at the location of the ETH/CU camp for the entire period was produced. The time series was then compared to the in situ data collected at the camp during the 1990 and 1991 field seasons.

The dates that correspond to sharp increases in cross-polarized gradient ratio are the same dates on which the mean liquid water content increased to approximately 1% by volume in the top meter of snow. These were identified as the dates of melt onset at the ETH/CU camp. According to the in situ measurements, the melt threshold was found to be XPGR = −0.0158. XPGR values above this threshold indicate that the pixel is representative of a wet region in the snow, while values below are consistent with a dry snow.

This value of 1% in the top meter is not a definite or exact value because after the top several centimeters reach 2% or greater liquid water content, the emission depth is only on the order of 2 cm for 37 GHz and approximately 8 cm for 19 GHz (Ulaby et al. 1986); consequently, the wetness characteristics below the surface are of little influence on the overall signal. Studies by Davis et al. (1987) show that emission at 35 GHz is virtually at its asymptotic blackbody limit with 5%–6% liquid water content in the top 3 cm of snow; thus, the threshold–wetness relationship is arbitrary. The criterion of 1% mean wetness in the top meter of snow was chosen for consistency with the analysis of Mote and Anderson (1995) and will facilitate comparisons between the two methods. This and other limitations of the method are discussed further in section 3e.

Since the field data are available only for one site, it is not known for certain whether these values are site specific. However, because the metamorphic processes during melt are the same throughout the melt region, it is assumed that the threshold does not vary with location. This assumption is supported by comparisons of time series from several locations on the ice sheet in different regimes of highly contrasting temperature characteristics (Abdalati and Steffen 1995): the ETH/CU camp, location A in Fig. 1 (79°N, 25°W), and location B in Fig. 1 (62°N, 43°W). These time series, which are plotted and discussed in more detail in Abdalati and Steffen (1995), show that the XPGR values during winter months are clearly below the threshold, while those of summer months are predominantly above it. For this reason, the threshold is believed to provide a sufficient distinction between wet and dry conditions throughout the melt regions.

In a previous application of the XPGR method (Ab-

dalati and Steffen 1995), an XPGR threshold consistent with 0.5% water content was used. This was sufficient to provide a classification based on SSM/I observations, but the signal-to-noise ratio for the SMMR data was too low for the useful application of the 0.5% criterion. The ability of microwave radiometers to detect water at the time of the development of the SMMR instrument was limited to nearly 1% liquid water content (Stiles and Ulaby 1980). For the sake of consistent analysis over the entire time period, a criterion of 1% was used for the SSM/I as well as the SMMR data. Also, as mentioned above, this criterion is consistent with that of Mote and Anderson (1995).

Once the threshold was established, all available SSM/I daily brightness temperatures for every pixel location on the ice sheet were examined. Areas with XPGR values above the threshold on a given day were classified as experiencing melt on that particular day, while those with values below were classified as dry. In this way, the areal extent of melt for each day of SSM/I coverage was determined, and mean monthly melt extent was calculated for the ''melt months'' (June, July, and August) of each year. Also determined were the interannual variations in melt extent.

c. SMMR analysis

The transition from one instrument to another requires careful analysis of the relative calibrations between the two for data consistency. To account for operational and instrumental differences between the SSM/I and SMMR instruments, the calibration coefficients of Jezek et al. (1991) were applied. However, the ice sheet melt has a diurnal cycle, and the two platforms have very different crossover times, which complicates the analysis.

The *Nimbus-7* satellite on which SMMR was flown had an ascending equatorial crossing time of shortly before noon and a descending crossing time of a little before midnight (12 h later). Given that the orbital period was approximately 100 min, the offset for passage directly over Greenland is approximately 20 min (after equatorial crossing on the ascent, and before equatorial crossing on the descent). The DMSP *F-8* satellite, which carries the first SSM/I sensor crosses the equator at about 0600LT on ascent and 1800LT on descent, with the same offsets as SMMR for Greenland crossover. As a result, observations of the Greenland ice sheet are made near local noon and midnight by the SMMR, and around 1800LT and 0600LT by the SSM/I.

In the southernmost latitudes of the ice sheet, the daily averaged brightness temperatures are simply an average of a single ascending observation and a single descending observation. In the northern portions of the ice sheet where the latitudinal circumference is smaller, the daily averaged brightness temperatures are comprised of six observations, three from ascending passes, and three from descending passes. This occurs because the conical scanning geometry and relatively wide swaths of the instruments allow for the sensing of a target at passes other than one that is most directly above the target. As a result, the pass preceding the one closest to the target's zenith, and the pass following it are also included in the averaging. However, since the orbital period is on the order of 100 min, the resulting values are clustered around the time of the direct overflight (being offset by not more than 100 min in either direction). Consequently, the daily averages represent averages of scans clustered around local noon and local midnight for the SMMR, and 0600 LT and 1800 LT for the SSM/I (within plus or minus 100 min in each case).

At the same time the melt undergoes a diurnal cycle, which peaks in the mid- to late afternoon (between 3 and 5 P.M. local time). At the time of onset, the melt period may last only a few hours, and as it becomes better developed, the melt period lasts longer (up to 24 h in the saturation and ablation zones). The same is likely to be true as the refreeze occurs—areas that are frozen for most of the day may be in the melt state for a few hours in the mid- to late afternoon. Considering this diurnal cycle, the magnitude of the emission increase as dry snow becomes wet, and the different crossover times of the instruments, it is reasonable to believe that the *F-8* SSM/I, with scans that occur closer in time to the strongest melt period, would detect more melt events than would the SMMR with scans further removed in time from the peak melt period. Consequently, in order to ensure consistency over the coverage period, an XPGR threshold needs to be applied to the SMMR data that is different from that of the SSM/I. This threshold should be lower than that of the SSM/I instrument.

To determine this threshold, an additional step of geophysical parameter matching was taken. During the overlapping coverage period (9 July–20 August 1987), and after applying the SMMR/SSM/I regression coefficients, the XPGR was calculated for both the SSM/I and SMMR observations. A new threshold for the SMMR data was then determined, which yielded the same melt areas (to within 6%) as those identified by the SSM/I data. In this way, the effects of diurnal differences are minimized. This new threshold is XPGR $= -0.0265$, and it is used as the melt criterion for the entire SMMR dataset.

In addition, the signal-to-noise ratio of the SMMR instrument is not as high as that of the SSM/I. The SMMR time series of the XPGR shows much more variability for consecutive coverage days than does the SSM/I. To reduce the effects of the noisy signal, a smoothing function was applied to the SMMR data. This function was a 5-day running mean, during two of which the instrument was inactive. In other words, the value of the brightness temperatures used on any given day is an average of the scans on that day plus those on the two nearest days of coverage—one from 2 days before the day examined and one from 2 days after. Such a smoothing reduces the temporal resolu-

tion, but has a negligible impact on the seasonal/interannual studies.

d. SSM/I F-11 *analysis*

The *F-11* instrument, like the *F-8*, has dusk/dawn crossover times with the ascending pass occurring at the equator at approximately 1730LT, and the descending pass occurring at 0530LT. Therefore, after accounting for instrumental differences between the two instruments, the same threshold, that is used for the *F-8* data, XPGR$=-0.0158$, should also be applicable to the *F-11* SSM/I data. Comparisons between the in situ data from the ETH/CU camp for the years 1993 and 1994 show that this threshold is valid, which further increases our confidence in the threshold selection.

One slight discrepancy that does arise, however, is that in 1994, there are several brief incidents in which the melt threshold is exceeded prior to melt onset. In other words, there apparently exist a few false melt signals. These occurred during camp occupation when a severe weather system passed that deposited snow. The presence of this system is believed to be the cause for this false melt signal, and, as explained in section 3f below, these events are of short duration and should not alter the melt statistics significantly.

e. Melt/threshold relationship

As previously noted, the thresholds are somewhat arbitrary because the depth and vertical stratification of water within the snow are variable. Consequently, a particular value of brightness temperature or combination thereof does not reflect a unique water content. In other words, a deep snow may have a low water content on average, but the surface could be very wet, as would be the case in the advent of a warm system passing through a region of the ice sheet. Alternatively, a shallow snowpack may be more uniformly wet, due to slower melt processes, such as purely radiatively driven melt, and may exhibit the same melt signal as in the previous example. Both can have very different wetness characteristics and mean water content percentages, yet they may still give the same signal.

A second complication arises because the spatial variability of the melt is very high even on small scales. Slight topography variations result in uneven heating in areas of the snow and variable temperature and density structure. As a result, melt is not horizontally uniform. The in situ measurements were taken in a vicinity believed to be typical or representative of the camp area; however, the variability of snow water content can be high within a pixel. Sample measurements in the field show variability as high as 3% water content over as little as 10-m distance; thus, no exact correlation can be made between the in situ point measurements and the 25-km pixel grid.

However, the data do lend themselves to the definition of a distinct threshold, which can be considered a boundary between dry and wet snow, and although the terms dry and wet may not be specific, the ability to monitor the areal extent of wet snow with a consistent algorithm from year to year is a useful observational tool in Arctic climate studies.

f. Atmospheric variability

In remote sensing of the high-latitude polar regions, atmospheric effects are very small at microwave frequencies and are often neglected (Massom 1991). This is especially true at the higher elevations of the ice sheet, where water vapor capacity is low, and the clouds that form are generally more transparent than the optically thick cumulus clouds near the coast. However, though it is only a very small part of the signal, emission from and attenuation by the atmosphere are a part of the apparent microwave brightness temperature, and is convolved with the melt signal.

None of the passive microwave melt methods to date have included variability in the atmosphere. Mote and Anderson (1995) explicitly incorporate the atmospheric contribution in their model, but changes in the atmosphere are not considered; thus, large changes in atmospheric optical thickness (i.e., cloud cover) are not accounted for. This generally has a greater impact on the low elevation areas than the higher, more cloud-free areas, but in all of these methods, atmospheric effects are assumed to be small in comparison to the change in emission due to wetness.

However, severe weather conditions and excessive water vapor in the atmosphere can significantly attenuate the surface emission. Thus, if melt exists under an optically thick atmosphere, the increased extinction can cause this melt to go undetected by the single-channel approaches. In the case of the XPGR parameter, the 37-GHz (0.81 cm) emitted energy is scattered more than the 19-GHz (1.55 cm) emission since its wavelengths are closer to the actual sizes of the scattering particles in the atmosphere (water, ice, and snow). As a result, the 37-GHz emission is more attenuated by the atmosphere than the 19-GHz emission. Consequently, the difference between the two increases under optically thick conditions such as those associated with clouds, water vapor, and precipitation. The normalization in the XPGR technique, however, mitigates this impact. A doubling of the atmospheric optical thickness is estimated to change the XPGR value 10% of the change associated with a 1% water content. Based on this first-order estimate, we assume that over large temporal and spatial scales, the atmospheric effects do not affect the trends significantly.

A more complete analysis would incorporate water vapor and cloud cover estimates over the ice sheet, but considering the severely limited means of estimating these parameters over the Greenland ice sheet, such analysis is not yet feasible.

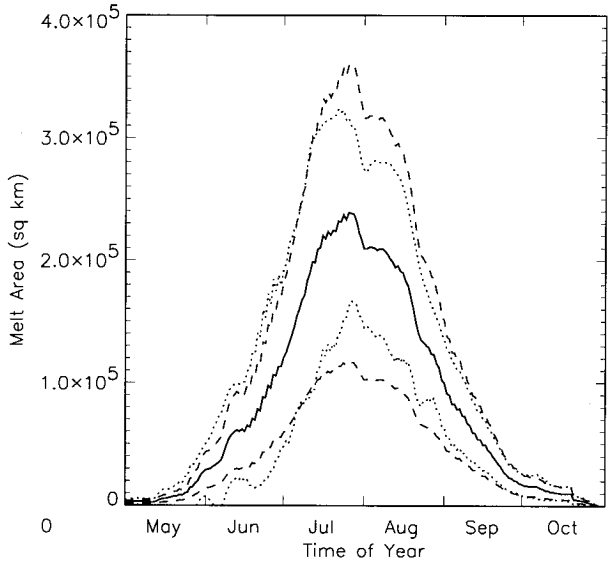

FIG. 3. The average spatial melt extent for the years 1979–94 (solid line), mean melt ± 1 standard deviation (dotted line), and melt area for 1°C temperature change (dashed line) in km² for the melt months of June, July, and August. The extent was calculated by determining the mean area coverage for these months in each year and then averaging these values over the entire coverage period.

g. Effects of bare ice

Bare ice emission on the ice sheet is assumed to be similar to that of thick lake ice and as such is relatively independent of frequency (Ulaby et al. 1986). As a result, the XPGR of a region in which the snow has completely melted is nearly zero, and is classified as melting snow. This assumption is supported by observations of late-season emission in the ablation zone. This phenomena leads to a late estimation of refreeze of exposed ice (until snow has fallen and remained frozen on the surface). However, since melt is considered only between the months of June and August, the assumption that the bare ice is wet is assumed to be of little consequence. Still, it is acknowledged as a limitation of the algorithm for melt assessment purposes.

4. Results and discussion

a. Seasonal melt cycle

The average extent of snowmelt for the years 1979–94 is shown in Fig. 3 along with the range of melt extent within one standard deviation of the average. Also shown are the melt areas associated with a heating or cooling of 1°C, which are discussed in section 4c below. The locations of melt for the primary melt months, June, July, and August, are depicted in Fig. 4. Melt onset begins at a limited number of coastal pixels in April and May and is very slight. In early June, the melt begins to spread, primarily around the region of Sondre Stromfjord and Jakobshavn but is still limited in areal extent. During mid- to late June, and the early part of July, the melt extent increases rapidly, as is indicated by the steep slope of the curve in Fig. 3. In late July, melt is at its maximum extent covering nearly the entire perimeter of the ice sheet, and most of the southern portion of the ice sheet (south of 68°N lat) with the exception of the high-elevation South Dome. After late July, refreeze begins to occur on the ice sheet and the areal extent of melt begins to drop off steadily until mid- to late September and then more gradually through October.

The area showing the most melt throughout the summer is the region along the west coast beginning at the southern tip of the ice sheet and extending north past Jakobshavn. This region is the first to show melt, the last to show refreeze, and remains wet, farther inland than most other locations (Figs. 4a–c). This may most likely be attributable to the gentle slope on the western side of the ice sheet, the greater radiation intensity at the lower latitudes as compared to the higher ones, and possibly the influence of the warm dry continental air mass approaching from Canada, which dominates the summer circulation (Ohmura and Reeh 1991). Another area of extensive melt is the northeast portion of the ice sheet near Danmarkshavn and Nord. This region also has a very gentle slope and is a low elevation (900 m above sea level). Subsequently, more melt would be expected in this area.

A significant characteristic of Fig. 3 is the skewness, or asymmetry about the peak. This results from a combination of two factors: 1) the differing emission depths for the two frequencies and 2) the fact that melt and refreeze of the snow both occur from the top down (i.e., first near the surface and then progressing deeper into the snow).

For dry snow near its melting point, 19-GHz radiation is emitted primarily in the top 2.5 m of the snowpack and at 37 GHz, most of the emission is from the top 30 cm (Ulaby et al. 1986). When melt begins near the surface, however, the effective emission depth decreases considerably to approximately 10 cm for a 1% liquid water content (Ulaby et al. 1986) for both 19 and 37 GHz. That is to say that more of the signal comes from the snow near the surface when the snow is wet than when the snow is dry. This occurs because in the case of dry snow, the energy can pass through the air between the snow grains with little or no extinction. As the space between the snow grains fills with water, nearly all of the energy that passes between the grains is absorbed by the water. With this increased extinction, the effective emission depth, defined as the inverse of the extinction coefficient, decreases.

During the spring and early summer, the snow is absorbing incident radiation and undergoing heating near the surface. The greater depths, which are primarily heated by conductive heat fluxes from the surface, respond more slowly. Therefore, during this time of year, the deeper snow is colder than the snow closer to the

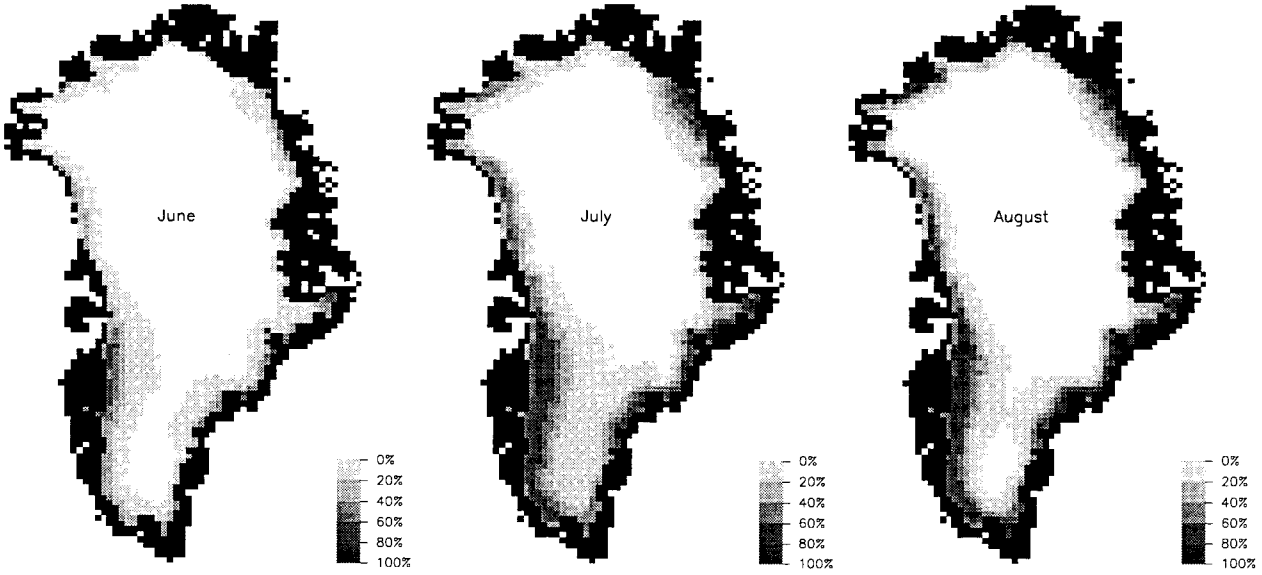

FIG. 4. Monthly melt maps of areal melt extent. The shaded areas are areas that experience melt in the month shown at least once in the period from 1979 to 1994, and the darkness indicates what percentage of the month (averaged over the time series) the pixel was wet. Light shading indicates a low wetness frequency, and dark shading indicates a high frequency of melt. The white areas represent the dry snow areas, and the black areas are regions of Greenland that are not fully covered by the ice sheet.

surface. When the snow becomes wet, the change in emission depth of the 19H results in a higher effective physical temperature [T_p in Eq. (1)] and therefore increases brightness temperature. Coupled with the sharp increase in emissivity of wet snow, the effects on brightness temperature are further increased. The same holds true for 37V, but the difference is not as great, since the change in emission depth is less. As a result, XPGR method is particularly sensitive to the onset of melt in spring, since it occurs near the surface.

During refreeze, the differing penetration depths act to prolong the detection of melt until the subsurface snow has refrozen. When the surface begins to refreeze, more of the 19H emission comes from below the surface than does the 37V emission. Consequently, when warmer wet snow lies beneath colder frozen snow, the XPGR signal indicates melt. This becomes problematic when the melt state of the surface is desired. For such an application, the method of Mote and Anderson (1995) is better suited. But for climatological investigations and snow structure modeling, knowledge of the subsurface characteristics, and the time of refreeze of the surface and subsurface snow, are important. For example, the passing of a cold front in late summer, which may act to refreeze the surface while the subsurface remains wet, will not be classified as dry until the snow is frozen at greater depths. In this way, the climate signal is more stable and less susceptible to surface variations and tracks wet snow through its complete cycle.

The differing penetration depths and the ''top down'' occurrence of melt cause the XPGR method to be highly sensitive to surface melt at the onset, yet not very sensitive to surface refreeze. For these reasons, the full extent of melt, and a melt climate signal, can be closely monitored without much influence from short-term refreeze events.

b. Melt extent

A full composite of the spatial melt extent and the percentage of melt days is shown in Fig. 5. The most active regions of the ice sheet are in the southern portion of the ice sheet (south of 68°N). These show the greatest variability in areal melt extent over the time period, while the more northern perimeter regions fluctuate little. The former areas are influenced in the summer by the Atlantic Ocean (Ohmura and Reeh 1991) and thus are affected by variations in circulation, temperatures, and extent of the Icelandic low.

The maximum melt areas depicted in Fig. 5 follow the same general contours as the facies classification map of Benson (1962), however, they are not as extensive. The Benson map indicates melt at higher elevations than are detected by the XPGR method. This may be due to the fact that Benson's estimates were based on studies of numerous snowpits dug between 1952 and 1955 (Benson 1962). The time period covered by Benson's data, which dated back to 1937 (Benson 1962), may have been anomalously warm or in a different climate regime.

In addition, the binning into daily averages may prevent the detection of some brief afternoon melt events by averaging them in with the nighttime brightness

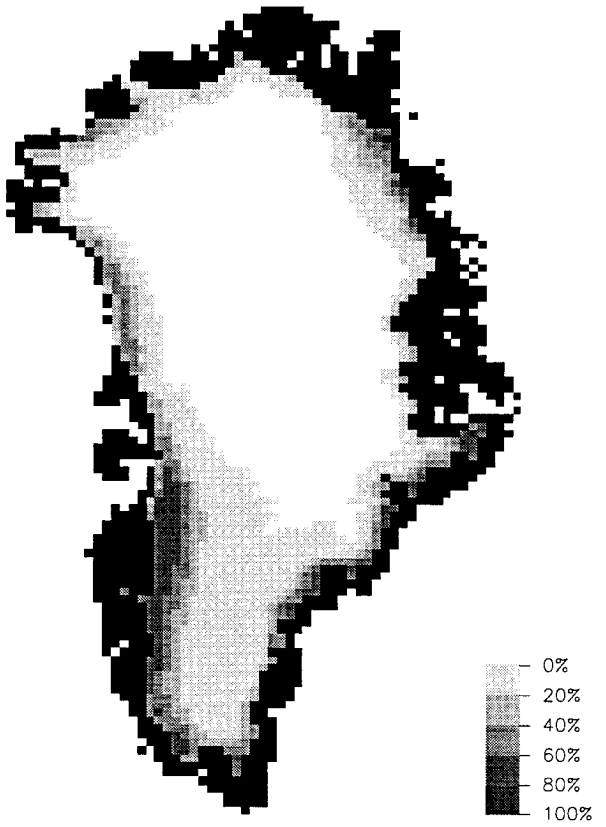

FIG. 5. The 1979–94 composite of melt. The shaded areas are areas that experience melt during the months of June, July, and August at least once in the period from 1979 to 1994. The different shades of gray indicate the percentage of time throughout the coverage period that the pixels experienced melt during these 3 summer months. The white areas represent the dry snow areas, and the black areas are the locations of pixels that are not fully covered by the ice sheet.

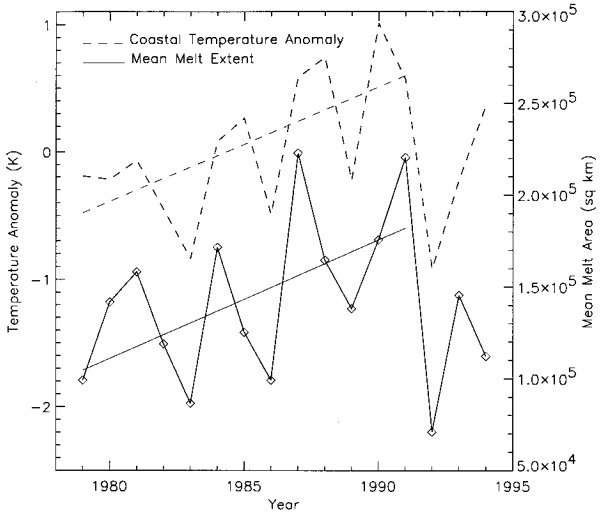

FIG. 6. Interannual variations in mean melt extent (average area for the months of June, July, and August of each year) as determined by the XPGR classification technique for the years 1979–94 (solid line). The years 1978–91 show a 4.4% increase in areal melt extent, which is consistent with the increase observed by Mote and Anderson (1995), though slightly greater (Mote and Anderson reported a 3.8% increase). In 1992, following the eruption of Mt. Pinatubo, the melt area decreased considerably before continuing to rise again in 1993 and 1994. Also shown (dashed line) are the coastal temperature anomalies from the six climate stations shown in Fig. 1 for the same time period. Temperatures also dropped significantly after the Pinatubo eruption.

temperatures of the refrozen surface. As a result, area melt extent may be slightly underdetected. However, in the future, this analysis can be repeated using Equal Area SSM/I Earth Grid (EASE-Grid) data when they become available, which will be divided into descending and ascending passes, thus eliminating the averaging in of the cold nighttime brightness temperatures.

It is also likely that the melt facies classification of Benson differs from the satellite-derived estimate because the criterion for ''melt'' differs. Satellite-observed melt classification would not necessarily be identical to that determined from pits and snow layers. What is most important for climate monitoring, however, is the consistency of the technique, and the XPGR method provides a consistent long-term assessment of the melt conditions on the ice sheet. This monitoring technique will be applicable as long as there are SSM/I (or similar) instruments in operation.

c. Interannual variations

The interannual variations of mean melt extent on the ice sheet are shown in Fig. 6. Also shown are the interannual variations in mean summer temperatures (the mean of the period 1 June–31 August) based on climate data from several stations along the coast. These datasets were obtained from the National Center for Atmospheric Research (NCAR) in Boulder, Colorado. The station locations are Thule, Sondre Stromfjord, Godthab, Julianehab, Danmarkshavn, and Angmagssalik (see Fig. 1). There were datasets available from additional stations, but the six listed were the most comprehensive. Three of the stations—Sondre Stromfjord, Godthab, and Julianehab—are located close to one another in comparison to the others, along the southwest coast of Greenland. To avoid a bias to this area, the three were averaged and treated as one value before being averaged in with the other coastal station temperatures.

Two features stand out in Fig. 6. The first is the drastic increase in melt extent between 1979 and 1991. This increase is 4.4% per year, which is slightly higher than the 3.8% per year reported by Mote and Anderson (1995). This increasing melt trend is consistent with the coincident warming trend during the years 1979–91, with a correlation coefficient $R = 0.78$. The temperature and melt correlations suggests that a 1°C temperature increase is accompanied by an increase in melt area of 73 000 km^2, which compares quite well to the 79 000 km^2 estimated by the slope and lapse rate calculation.

This additional 73 000 km^2 represents a 52% increase over the average melt area.

As illustrated in Fig. 3, the 52% increase results in a melt area that is within the 1 standard deviation of the natural variability for the early and late parts of the melt season (before the end of June and after late September), but it is well outside of this range in July and August. Thus, the melt associated with a warming of Greenland of as little as 1°C nearly exceeds the natural variability of the ice sheet melt variation. Since an average increase of more than 1.1°C was observed between 1979 and 1991, such a situation is not unlikely in the greenhouse scenario. Therefore, greenhouse-related temperature increases can be expected to significantly increase the spatial extent of melt on the ice sheet.

The second notable characteristic of Fig. 6 is the sharp drop in mean melt extent and temperature in the year 1992 to the lowest values of the 16-yr time period. In June 1991 Mt. Pinatubo erupted spewing large amounts of aerosols (ash and sulfur dioxide) into the atmosphere. For the months and even years following the eruption, the effects of the increased aerosols and ''nuclear winter'' have been felt worldwide primarily as changes in temperatures and the associated effects (Halpert et al. 1994). The melt extent seems to be no exception. The increased aerosols reduced the amount of solar energy reaching the surface of the earth. It is quite feasible that this is the cause of the reduction in melt area. In the years following 1992, the increasing trend appears to resume.

5. Conclusions

Satellite measurements enable consistent long-term climate studies of the Greenland ice sheet. The XPGR technique identifies the seasonal cycle and interannual variations in melt on the Greenland Ice sheet. The 16-yr dataset indicates that the melt extent peaks in late July and recedes more slowly than it advances, in part because the method detects wet snow lying below dry snow. This subsurface melt detection can potentially be used in conjunction with a method more sensitive to surface conditions (e.g., Mote and Anderson 1995) to provide more information about the vertical wetness structure of the snow. The results also suggest that maximum melt occurs on the western coast, particularly in the southern part of the ice sheet, and that the areas most sensitive to melt variations are the lower latitude regions of the ice sheet.

There is a significant increasing trend in melt area of 4.4% per year from 1979–91. This corresponds well with the observed increase in coastal temperatures between 1979 and 1991 of 1.1°C. In 1992, this trend was disrupted, possibly by the eruption of Mt. Pinatubo, and after 1992, the melt area returned toward its higher levels. An additional 2 years of data should provide information as to whether the increasing melt trend observed prior to 1992 is resumed. Also, despite these post-Pinatubo variations, there appears to be a distinct relationship between temperature increases and melt area increases such that melt area increases by 52% for a 1°C temperature rise. Such a melt area increase is well outside one standard deviation of the natural variability of melt during the peak melt months of July and August. Thus, small changes in the Greenland climate are likely to result in large changes in the areal melt.

Using the XPGR method, melt conditions on the Greenland ice sheet can be monitored in space and time. Such capabilities are useful for understanding how the Greenland ice sheet responds to our changing climate. In the future, these melt conditions can be compared to such climatological conditions as atmospheric circulation, temperature, sea ice extent, etc., and they can be incorporated into climate models, thus providing a better understanding of the intimate links between the Greenland ice sheet, and the regional and global climates.

Acknowledgments. This research was supported by NASA Polar Program Grant NAWG-2158, and by the Swiss National Foundation for Scientific Research Grants 21-27449.89 and 20-36396.92. The authors would like to acknowledge the efforts of Dennis Joseph at NCAR, who provided the coastal climate station data. Also, we would like to thank Claire Parkinson and Jay Zwally for their insightful comments and suggestions, which improved the paper.

REFERENCES

Abdalati, W., and K. Steffen, 1995: Passive microwave-derived snow melt regions on the Greenland Ice sheet. *Geophys. Res. Lett.*, **22,** 787–790.

——, ——, C. Otto, and K. C. Jezek, 1995: Comparison of brightness temperatures from SSMI instruments on the DMSP F8 and F11 satellites for Antarctica and the Greenland Ice sheet. *Int. J. Remote Sens.*, **16,** 1223–1229.

Benson, C. S., 1962: Stratigraphic studies in the snow and firn of the Greenland Ice Sheet. U.S. Snow, Ice and Permafrost Research Establishment Research Rep. 70, 93 pp.

Davis, R. E., J. Dozier, and A. T. C. Chang, 1987: Snow property measurements correlative to microwave emission at 35 GHz. *IEEE Trans. Geosci. Remote Sens.*, **25,** 751–757.

Denoth, A., 1985: Static dielectric constant as a textural index of snow. *Ann. Glaciol.*, **6,** 203–206.

Halpert, H. C., G. D. Bell, V. E. Kousky, and C. F. Ropelewski, 1994: *Fifth Annual Climate Assessment.* National Atmospheric and Oceanic Administration, 111 pp.

Jezek, K. C., C. Merry, D. Cavalieri, S. Grace, J. Bedner, D. Wilson, and D. Lampkin, 1991: Comparison between SMMR and SSM/I passive microwave data collected over the Antarctic ice sheet. Byrd Polar Research Center Tech. Rep. 91-03, Ohio State University, Columbus OH, 62 pp.

Massom, R. A., 1991: *Satellite Remote Sensing of Polar Regions.* Belhaven Press, 307 pp.

Mätzler, C. H., and R. Hüppi, 1989: Review of signature studies for

microwave remote sensing of snowpacks. *Adv. Space Res.,* **9,** 253–265.

Mote, T. L., and M. R. Anderson, 1995: Variations in snowpack melt on the Greenland ice sheet based on passive microwave-measurements. *J. Glaciol.,* **41,** 51–60.

——, ——, K. C. Kuivinen, and C.M. Rowe, 1993: Passive microwave-derived spatial and temporal variations of summer melt on the Greenland ice sheet. *Ann. Glaciol.,* **17,** 233–238.

Ohmura, A., and N. Reeh, 1991: New precipitation maps for Greenland. *J. Glaciol.,* **37.**

Orvig, S., 1970: *Climates of the Polar Regions.* Vol. 14, *World Survey of Climatology,* Levier Publishing Company, 370 pp.

Ridley, J., 1993: Surface melting on Antarctic Peninsula ice sheet detected by passive microwave sensors. *Geophys. Res. Lett.,* **20,** 2639–2642.

Steffen, K., 1995: Surface energy exchange at the equilibrium line on the Greenland ice sheet during onset of melt. *Ann. Glaciol.,* **21,** 13–18.

——, W. Abdalati, and J. Stroeve, 1993: Climate sensitivity studies of the Greenland ice sheet using satellite AVHRR, SMMR, SSM/I, and in situ data. *Meteor. Atmos. Phys.,* **51,** 239–258.

Stiles, W. H., and F. T. Ulaby, 1980: The active and passive microwave response to snow parameters 1. Wetness. *J. Geophys. Res.,* **85,** 1037–1044.

Thomas, R. H., 1993: Ice sheets. *Atlas of Satellite Observations Related to Global Change.* R. J. Gurney, J. L. Foster, and C. L. Parkinson, Eds., Cambridge University Press, 385–400.

Ulaby, F. T., R. K. Moore, and A. K. Fung, 1986: *Microwave Remote Sensing.* Vol. 3, *From Theory to Applications,* Artech House, 1120 pp.

Warrick, R., and J. Oerlemans, 1990: Sea level rise. *Climate Change: The IPCC Scientific Assessment,* J. T. Houghton, G. J. Jenkins, and J. J. Ephrams, Eds., Cambridge University Press, 257–282.

Zwally, H. J., 1977: Microwave emissivity and accumulation rate of polar firn. *J. Glaciol.,* **18,** 195–216.

——, and S. Fiegles 1994: Extent and duration of Antarctic surface melting. *J. Glaciol.,* **40,** 463–476.